PROCEEDINGS B

royalsocietypublishing.org/journal/rspb

Research

Cite this article: Hu MY, Petersen I, Chang WW, Blurton C, Stumpp M. 2020 Cellular bicarbonate accumulation and vesicular proton transport promote calcification in the sea urchin larva. *Proc. R. Soc. B* **287**: 20201506. http://dx.doi.org/10.1098/rspb.2020.1506

Received: 25 June 2020
Accepted: 7 August 2020

Subject Category:
Development and physiology

Subject Areas:
physiology, cellular biology

Keywords:
biomineralization, primary mesenchyme cells, intracellular pH, vesicular pH, life-cell imaging, ocean acidification

Author for correspondence:
Marian Y. Hu
e-mail: m.hu@physiologie.uni-kiel.de

Electronic supplementary material is available online at https://doi.org/10.6084/m9.figshare.c.5095278.

THE ROYAL SOCIETY PUBLISHING

Cellular bicarbonate accumulation and vesicular proton transport promote calcification in the sea urchin larva

Marian Y. Hu[1], Inga Petersen[1], William Weijen Chang[1], Christine Blurton[2] and Meike Stumpp[2]

[1]Institute of Physiology, Christian-Albrechts-University Kiel, Hermann-Rodewaldstraße 5, 24118 Kiel, Germany
[2]Institute of Immunobiology, Christian-Albrechts-University Kiel, Am Botanischen Garten 1-9, 24118 Kiel, Germany

MYH, 0000-0002-8914-139X; MS, 0000-0001-7765-2996

The sea urchin embryo develops a calcitic endoskeleton through intracellular formation of amorphous calcium carbonate (ACC). Intracellular precipitation of ACC, requires HCO_3^-/CO_3^{2-} concentrating as well as proton export mechanisms to promote calcification. These processes are of fundamental importance in biological mineralization, but remain largely unexplored. Here, we demonstrate that the calcifying primary mesenchyme cells (PMCs) use Na^+/H^+-exchange (NHE) mechanisms to control cellular pH homeostasis during maintenance of the skeleton. During skeleton re-calcification, pH_i of PMCs is increased accompanied by substantial elevation in intracellular $[HCO_3^-]$ mediated by the Na^+/HCO_3^- cotransporter Sp_Slc4a10. However, PMCs lower their pH_i regulatory capacities associated with a reduction in NHE activity. Live-cell imaging using green fluorescent protein reporter constructs in combination with intravesicular pH measurements demonstrated alkaline and acidic populations of vesicles in PMCs and extensive trafficking of large *V*-type H^+-ATPase (VHA)-rich acidic vesicles in blastocoelar filopodial cells. Pharmacological and gene expression analyses underline a central role of the VHA isoforms *Sp_ATP6V0a1*, *Sp_ATP6V01_1* and *Sp_ATPa1-4* for the process of skeleton re-calcification. These results highlight novel pH regulatory strategies in calcifying cells of a marine species with important implications for our understanding of the mineralization process in times of rapid changes in oceanic pH.

1. Background

To generate $CaCO_3$ shells and skeletons, calcifying organisms must accumulate Ca^{2+} ions and dissolved inorganic carbon (e.g. HCO_3^- and CO_3^{2-}) by cellular transport mechanisms [1–3]. During this mineralization process, protons are liberated that need to be removed from the calcification front to allow further mineral precipitation [1]. Thus, efficient trans-membrane transport systems that regulate pH and deliver calcification substrates to the calcification front are a fundamental requisite of all calcifying systems with the underlying mechanisms not clearly understood. This mechanistic knowledge will have important implications for our understanding of the mineralization process in marine calcifiers, and their ability to cope with rapid changes in the seawater carbonate system due to the phenomenon of ocean acidification (OA) [4].

For more than a century, the sea urchin larva has been used by biologists to study mechanisms and gene regulatory networks underlying the formation of an elaborate calcitic endoskeleton [5–7]. The larval skeleton is produced by primary mesenchyme cells (PMCs) that form syncytial cables through cell fusion surrounding the skeletal rods [8,9]. Amorphous calcium carbonate (ACC) is produced in intracellular vesicles of PMCs and is exocytosed into the luminal space of the syncytial cables to promote skeletal growth [10,11]. A range of matrix proteins that regulate crystal nucleation, ACC stabilization and recruitment of Ca^{2+} ions

[12–14] are required for the proper development of the larval skeleton. The current model denotes that Ca^{2+} is acquired by the PMCs from the highly permeable primary body cavity [15] through endocytosis of seawater-like fluids [3,16]. Carbon isotope studies demonstrated that approximately 60% of dissolved inorganic carbon (DIC) is used to build the larval skeleton derived from metabolic CO_2, whereas the remaining 40% are acquired from the seawater [1]. Here, the SLC4 family bicarbonate transporter *Sp_SLC4a10* has been identified to be critically involved in the cellular accumulation of HCO_3^- from the seawater [17]. By using a combination of metabolic CO_2 as well as HCO_3^- from the seawater as a DIC source, 1.6 moles of H^+ are liberated for each mole of $CaCO_3$ precipitated that need to be removed from the site of calcification to allow further precipitation. This requires acid fluxes that are comparable to those found in acid-secreting cells including osteoclasts, renal tubular cells and gastric parietal cells [18]. Thus, the present work aims at identifying acid–base transport mechanisms in PMCs that are critically involved in the calcification process of the sea urchin larva.

In the sea urchin larva, potential candidates for proton transport including Na^+/H^+-exchangers (NHEs), *V*-type H^+-ATPases (VHAs) and a putative H^+/K^+-ATPase (HKA) have been described [17,19,20]. Four NHE isoforms are found in the sea urchin genome of which only two are expressed in PMCs [21]. Of these two isoforms only *Sp_SLC9a2* is expressed in endodermal tissues and PMCs and increased expression levels were detected under acidified conditions resembling near-future OA scenarios [22,23]. A pharmacological approach using the specific HKA inhibitor SCH28080 demonstrated decreased calcification through impaired PMC fusion accompanied by reductions in the pH_i of PMCs [20]. Despite this pharmacological evidence for the existence of the HKA in PMCs, the gene for the HKA has not been found in basal deuterostome genomes, including those of sea urchins, hemichordates and ascidians [19]. Seven VHA V_0 subunit isoforms are found in the sea urchin genome database, of which all are expressed in PMCs [21]. Despite their existence in PMCs and an upregulation of some of these isoforms during skeletogenesis it remains unknown whether a proton pump expressed by PMCs contributes to the calcification process or serves other cellular functions.

This work aims to identify proton transport processes in PMCs that are of fundamental importance in the biomineralization process. Here, we first address differences in pH regulatory mechanisms of PMCs with a special focus on Na^+/H^+ exchange and HCO_3^- transport mechanisms. Intracellular as well as intravesicular pH measurements were performed to characterize pH conditions in these compartments during skeleton re-calcification, suggesting an important contribution of bicarbonate accumulation and vesicular pH homeostasis in the calcification process.

2. Results

(a) Na^+/H^+-exchange mechanisms in primary mesenchyme cells and their contribution to calcification

Pharmacological inhibition of H^+ transport mechanisms by 5-(N-ethyl-N-isopropyl)amiloride (EIPA) and Bafilomycin A1, targeting NHE and the VHA revealed a strong impact of EIPA on PMC pH regulatory capacities (figure 1*a–c*). The compensation reaction after removal of NH_4^+ was inhibited by 1 µM EIPA down to less than 10% compared to PMCs only exposed to the vehicle dimethyl sulfoxide (DMSO). EIPA inhibition followed a sigmoidal dose–response curve with an IC_{50} value of 0.066 µM (figure 1*d*). While 80% of PMCs ($n = 25$ larvae; 137 cells) significantly reduced pH regulatory capacities in the presence of 1 µM EIPA, 20% showed only a mild, non-significant response to the inhibitor (figure 1*a–c*). To assure the correct identification of PMCs, intracellular pH measurements were performed in combination with PMCs expressing the reporter construct *ALX1*-green fluorescent protein (GFP). This transcription factor serves as a marker for PMCs [24,25] and confirms that *ALX1* expressing PMCs indeed have differential sensitivities to EIPA (electronic supplementary material, figure S1). Compensation of an intracellular acidosis was insensitive to the VHA inhibitor Bafilomycin A1 at a concentration of 1 µM (electronic supplementary material, figure S2). Calcein pulse-chase experiments in combination with EIPA demonstrated a significant decrease in Ca^{2+} incorporation by 10% and 20% into the spicule in the presence of 0.1 µM and 1 µM EIPA compared to a control group only exposed to the vehicle DMSO (figure 1*e*). Here, it should be noted that EIPA has been demonstrated to inhibit macropinocytosis [26], and thus reductions in calcification rates under the inhibitor treatment may be a result of reduced Ca^{2+} uptake by vesicular pathways.

Our findings suggest that NHE proteins participate in the regulation of pH in PMCs and therefore we searched for potential gene candidates. A *Stongylocentrotus purpuratus* specific antibody designed against the sea urchin NHE-2 (Sp_SLC9a2) revealed a distinct signal in PMCs as well as in cells of the larval gut (figure 1*f*). In prism stage larvae (2 days post-fertilization (dpf)) Sp_SLC9a2 was localized to the developing gut. In early pluteus larvae (3 dpf) Sp_SLC9a2 protein was detected in sub-cellular compartments whereas in older larvae high concentration of this protein were found in the plasma membrane, cytosol as well as in the cytoplasmic sheath of PMCs covering the mature spicule (figure 1*f,g*). In pluteus larvae SP_SLC9a2 was colocalized with Sp_SLC4a10 (electronic supplementary material, figure S3). Negative controls using the immunization peptide demonstrated no unspecific binding of the antibodies and western blot (WB) analyses revealed major immune-reactivity with a protein in the predicted size range of 95 kDa (figure 1*h,i*).

In summary, we observed a significant role of NHEs in the pH regulatory mechanism of PMCs under resting conditions, and identified SLC9a2 as a potential candidate that mediates this function.

(b) pH_i regulatory capacities during skeleton re-calcification

To study pH regulatory dynamics in actively calcifying PMCs we used the re-calcification assay where the skeleton is dissolved and completely rebuilt within few days. To conduct the re-calcification assay we exposed pluteus larvae for 12 h to 2-(N-Morpholino)ethanesulfonic acid hemisodium salt (MES) buffered filtered natural seawater (FSW) adjusted to pH 6 which led to complete dissolution of the skeleton. After 2 days in FSW (pH 8.1) larvae started to rebuild their skeletons with most rapid re-calcification of the spicule between day 1 and day 3 (figure 2*a*). Skeleton re-calcification was initiated by a thin spicule in the mid-region of the body rod and was extended towards the anterior and posterior ends of the

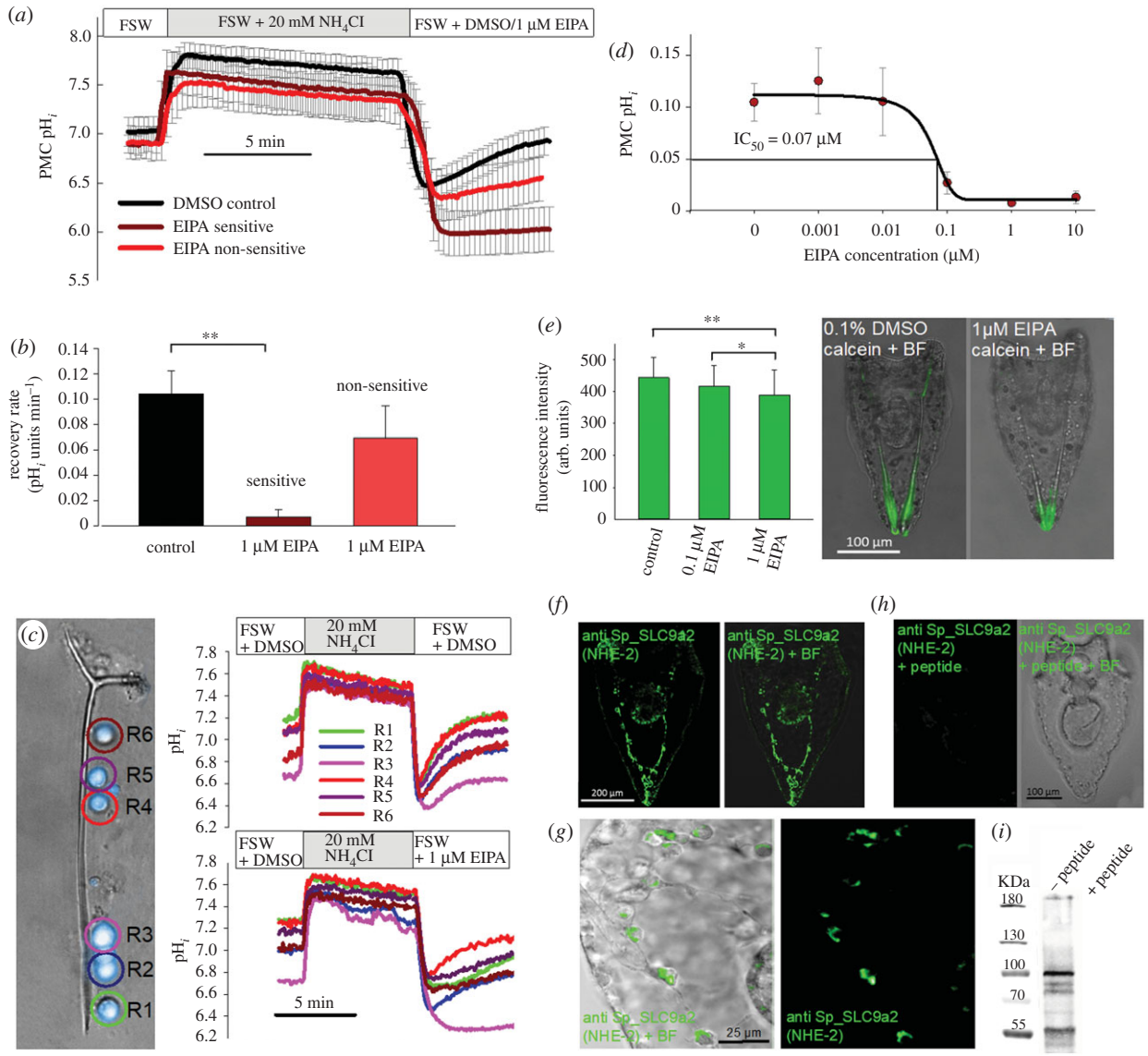

Figure 1. Pharmacological and immuno-histological evidence for Na^+/H^+ exchanger (NHE) dependent pH regulation in PMCs. (*a*,*b*) Intracellular pH measurements in combination with the ammonium pulse technique demonstrated differential sensitivities of PMCs to the NHE inhibitor EIPA ($n = 8$–11 larvae) (electronic supplementary material, figure S1). (*c*) Exemplary measurement of pH regulatory abilities of single PMCs sitting along one spicule. Real time traces of pH_i recordings in the presence of 0.1% DMSO (upper graph) or under 1 µM EIPA treatment (lower graph). (*d*) Dose–response curve for the recovery rate in the presence of different EIPA concentrations in EIPA sensitive cells ($n = 6$–9). (*e*) Calcein pulse-chase experiments in the presence of different EIPA concentrations. (*f*) Localization of the NHE-2 in PMCs of the sea urchin larva (4 dpf) using a custom made antibody raised against the sea urchin SP_SLC9a2 protein. (*g*) Higher magnification of SP_SLC9a2 immunoreactivity in PMCs of an early pluteus larva (3 dpf). (*h*) Peptide compensation assays are used as negative controls. (*i*) Western blot analysis demonstrates major immunoreactivity with a 100 kDa protein. All values are presented as mean ± s.e.m. Asterisks indicate significant differences (*$p < 0.05$; **$p < 0.001$). (Online version in colour.)

larva. This re-calcification often resulted in abnormal branching in the apex region of the regenerated spicule (figure 2*a*). After 6 days, re-calcification was completed with only slight irregularities in the spicule rods. pH_i regulatory capacities of PMCs during the re-calcification phase were measured by a direct CO_2-induced acidification using out-of-equilibrium seawater solutions (2.5%CO_2/pH 8.0) (figure 2*b*) and the ammonia pulse method (electronic supplementary material, figure S4). Under control conditions (no de-calcification) pH_i of PMCs was restored at a rate of 0.0041 ± 0.0003 pH units min^{-1}. During the early re-calcification phase (D1 + 2) pH_i regulatory capacities were dramatically decreased by −0.027 ± 0.004 and −0.038 ± 0.005 pH units min^{-1} compared to PMCs of control larvae (figure 2*c*). After 3 and 6 days of re-calcification PMC pH_i regulatory abilities almost recovered back to control conditions. During the re-calcification phase (D1 + 2) pH_i was significantly ($p = 0.003$) increased by 0.31 ± 0.07 and 0.22 ± 0.09 pH units. This increase in pH_i was accompanied by an elevation in intracellular HCO_3^- levels calculated based on pH_i and literature values for intracellular pCO_2 of marine invertebrates [27].

To address the molecular mechanisms underlying the differences in pH_i regulation during skeleton re-calcification we blocked putative ion transporters using a pharmacological approach. The negative slope of pH_i min^{-1} during the CO_2 induced acidosis in re-calcifying PMCs was even further decreased by the addition of 500 µM 4,4′-diisothiocyano-2,2′-stilbenedisulfonic acid (DIDS) and 1 µM Bafilomycin inhibiting bicarbonate transporters and VHAs, respectively (figure 2*f*,*g*). However, in this re-calcification stage 1 µM EIPA had no effect on pH regulatory abilities of PMCs (figure 2*h*). Comparisons of compensatory slopes during acidification by 2.5% CO_2 in control PMCs, control PMCs exposed to 1 µM EIPA and re-calcifying PMCs demonstrate similarly decreased pH_i

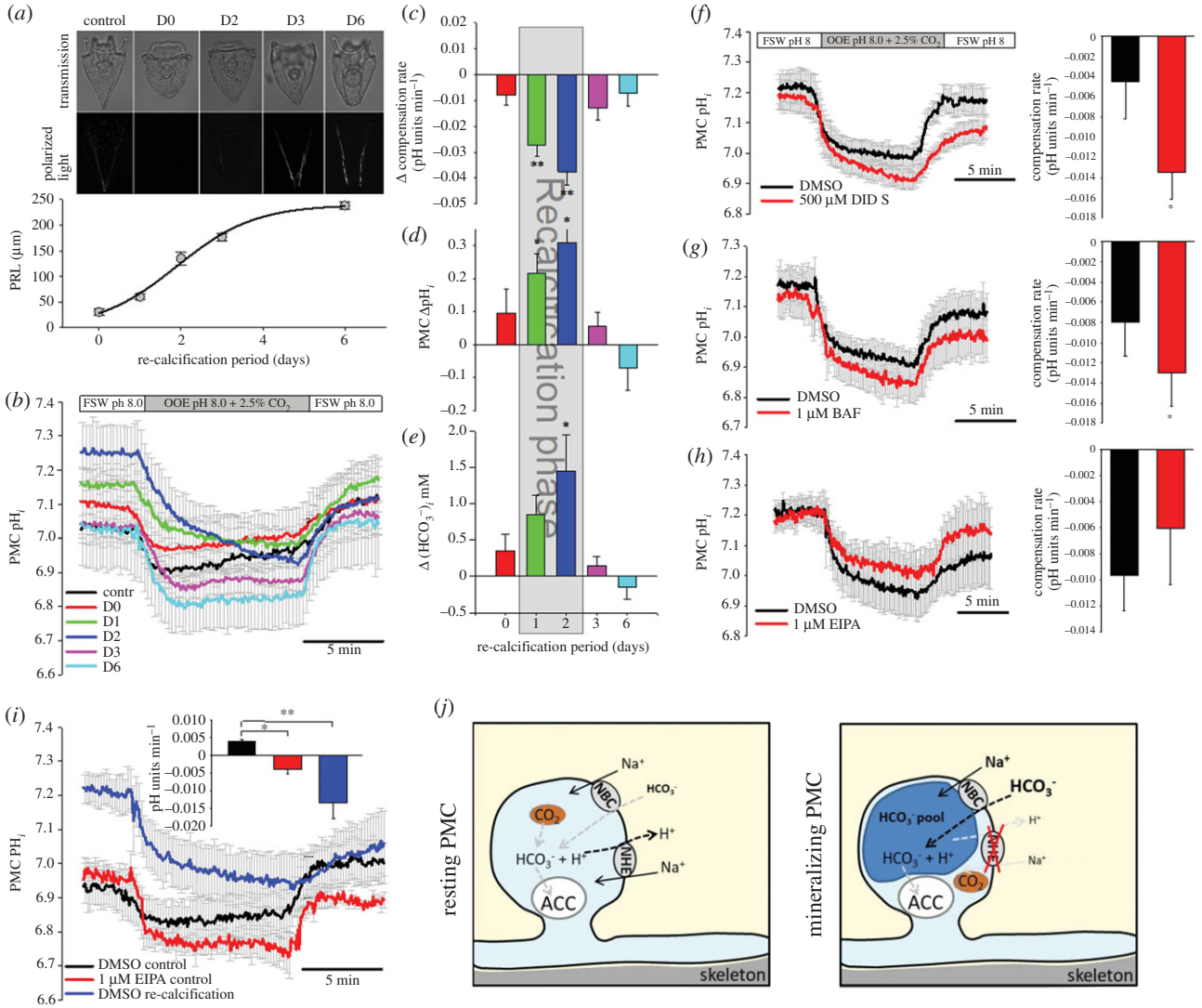

Figure 2. pH regulatory capacities of PMCs during skeleton re-calcification. (*a*) Re-calcification of the larval skeleton after dissolution within 6 days indicated by the primary rod length (PRL) ($n = 5$). (*b*) CO_2 pulse experiments using out of equilibrium solutions (OEE; 2.5% CO_2 and pH 8.0) were used to characterize cellular pH regulatory capacities at different time points of re-calcification ($n = 8$–10). Determination of pH regulatory capacities (*c*), baseline intracellular pH (pH_i) (*d*) and calculated intracellular $[HCO_3^-]$ (*e*) along the re-calcification period. Sensitivity of pH regulatory capacities to the HCO_3^- transport inhibitor DIDS (*f*) the *V*-type H^+-ATPase inhibitor Bafilomycin (BAF) (*g*) and the NHE inhibitor EIPA (*h*) during re-calcification ($n = 5$–6). (*i*) Comparison of pH regulatory capacities of PMCs under control conditions, in the presence of EIPA and in the re-calcification phase ($n = 5$–6). Schematic model illustrating shifts in transporter activity in resting and mineralizing PMCs. Values are presented as mean ± s.e.m. Asterisks denote significant differences (**$p < 0.001$; *$p < 0.05$) between treatments. (Online version in colour.)

regulatory abilities in re-calcifying and EIPA treated control PMCs (figure 2*i*). DIDS inhibited pH_i regulatory capacities during the CO_2 pulse in control larvae leading to a decrease in the compensatory slope from 0.004 ± 0.001 to -0.016 ± 0.002 pH units min^{-1} in control and DIDS treated PMCs, respectively (electronic supplementary material, figure S5*a*,*b*). Bafilomycin had no effect on pH_i regulatory capacities using the CO_2 pulse method (electronic supplementary material, figure S5*c*,*d*). Figure 2*j* depicts differences between resting and calcifying PMCs that have an elevation in intracellular HCO_3^- levels accompanied by a reduction in sensitivity to the NHE inhibitor EIPA. This suggests a minor contribution of NHEs to the calcification process.

(c) Interaction of blastocoelar filopodial cells with primary mesenchyme cells and characterization of vesicular pH

During the phase of skeleton re-calcification, the number of large blastocoelar filopodial cells (BFCs) highly increased in the extracellular space of the primary body cavity and BFCs interacted with PMCs and their syncytium (figure 3*a*). Tagging of PMCs using the *ALX1*-GFP bacterial artificial chromosome (BAC) demonstrates that BFCs are not of skeletogenic mesenchyme origin. BFCs endocytose fluorescence labelled dextrans into large vesicles that are transported by the extensive filopodial network (figure 3*b*, electronic supplementary material, videos S1 and S2). The dynamic network of filopodial cells is strongly associated with PMCs by membrane interactions of both cell types (figure 3*a*–*c*). Because BFCs are strongly associated with PMCs, pH regulatory capacities as well as vesicular pH determinations of these two cell types were compared to see if their physiology shows similar responses during skeleton re-calcification or not. pH_i recordings performed during the re-calcification process demonstrated decreased pH_i regulatory capacities and increased cytosolic pH in PMCs (figure 3*d*,*e* R2–R6) whereas large vesicle-rich BFCs (figure 3*d*,*e* R1) have significantly ($p < 0.001$) higher pH_i regulatory capacities of 0.005 ± 0.0003 pH units min^{-1} and a pH_i of 6.92 ± 0.05 (figure 3*f*).

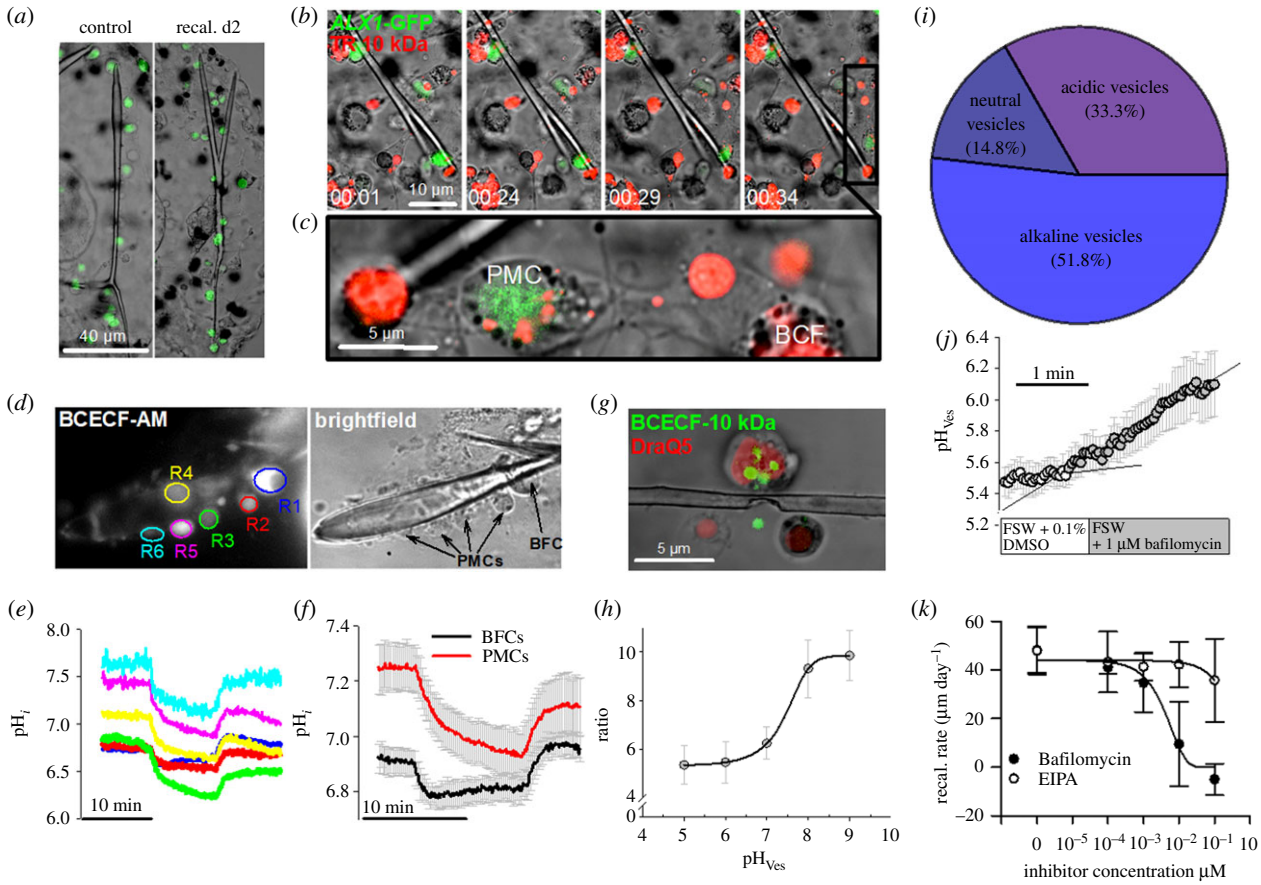

Figure 3. pH_i regulatory abilities of blastocoelar filopodial cells (BFCs) and characterization of vesicular pH during skeleton re-calcification. (*a*) During re-calcification a large number of BFCs (indicated by arrows) occur in the extracellular matrix of the primary body cavity that are associated with the regenerating skeleton. BFCs are of non-PMC origin as indicated by the expression of the GFP tagged skeletogenic mesenchyme cell marker *ALX1*. (*b*) Confocal time-lapse recording of BFCs that endocytosed TexasRed (TR) 10 KDa dextran (red) into large vesicles. Arrow indicates a BFC that migrates and attaches to a PMC. (*c*) BFCs attach to PMCs and transport endocytosed vesicles across their filopodial network (electronic supplementary material, videos S1 and S2). (*d*,*e*) BCECF-AM loaded cells along a regenerating spicule for the determination of pH_i regulatory abilities of BFCs (R1) and PMCs (R2-R6) after 2 days (D2) of skeleton re-calcification using the CO_2 pulse method. (*f*) Comparison of pH regulatory capacities of BFCs and PMCs during re-calcification (D2) ($n = 6$). (*g*) Determination of intravesicular pH (pH_{Ves}) in PMCs and BFCs using endocytosed BCECF-FA conjugated with a 10 kDa dextran molecule. (*h*) Calibration of pH_{Ves} in the presence of nigericine and 150 mM [K^+] seawater solutions adjusted to different pH values ($n = 3$–4). (*i*) Quantification of alkaline (>pH 7.5), neutral (pH 6.5–7.5) and acidic (pH < 6.5) vesicles ($n = 27$) from PMCs. (*j*) Inhibition of vesicular acidification in large endocytotic vesicles of BFCs by the *V*-type H^+-inhibitor Bafilomycin ($n = 4$). (*k*) Re-calcification rates measured as skeletal rod-growth per day under different concentrations of Bafilomycin and EIPA ($n = 4$). Values are presented as mean ± s.e.m. (Online version in colour.)

The membrane-impermeable pH-sensitive dye BCECF-FA conjugated to a 10 KDa dextran is taken up into PMCs by endocytosis and localized within vesicles (figure 3*g*). Calibration of the dye in intracellular vesicles using a high potassium solution in combination with the H^+/K^+-ionophore nigericine resulted in a sigmoidal function between 440 and 486 nm fluorescence ratio and intravesicular pH (figure 3*h*). Determination of intravesicular pH in PMCs of pluteus larvae under control conditions (no re-calcification) demonstrated a share of 51.8% alkaline (>pH 7.0), 14.8 neutral (pH 6.5–7.0) and 33.3% acidic (<pH 6.5) vesicles (figure 3*i*). The pH of large vesicles in BFCs was acidic (pH 5.5 ± 0.1) and vesicular acidification was sensitive to the VHA inhibitor Bafilomycin (figure 3*j*). Re-calcification capacities determined by the growth rate of the primary rod after skeleton dissolution demonstrated a full inhibition of skeletal re-calcification in the presence of 1 µM Bafilomycin (figure 3*k*). By contrast, re-calcification was not impacted by EIPA at a maximum concentration of 1 µM (figure 3*k*). After the inhibitor treatments, all larvae were alive and showed no signs of collateral effects (i.e. swimming ability, swallow movements) by the inhibitors up to a concentration of 1 µM.

(d) Modulation of acid–base transporters during skeleton re-calcification

Our findings indicate that Na^+/HCO_3^- co-transporters (NBCs) and NHEs might play a role in the regulation of the re-calcification process. We, therefore, measured the change in the mRNA level of relevant genes during this process. During re-calcification positive immunoreactivity of the Sp_Slc4a10 (NBC) antibody was found throughout PMCs and their syncytial cables (figure 4*a*). NBC protein levels increase by 2.27-fold and 1.79-fold at the time points D0 and D1 of re-calcification, respectively (figure 4*b*). Protein concentrations return to control levels at D2 and 3 of skeleton re-calcification. Quantitative polymerase chain reaction (qPCR) analysis of putative calcification related genes coding for ion transporters and pumps revealed dynamic changes along the re-mineralization period of 3 days (figure 4*c*). mRNA levels of *Sp_Slc4a10* (*NBC*) were significantly increased throughout the entire re-mineralization period with highest expression levels at D2. By contrast *Sp_Slc9a2* (*NHE*) mRNA levels were not significantly affected during the re-calcification phase. mRNA expression revealed differential expression patterns between the seven

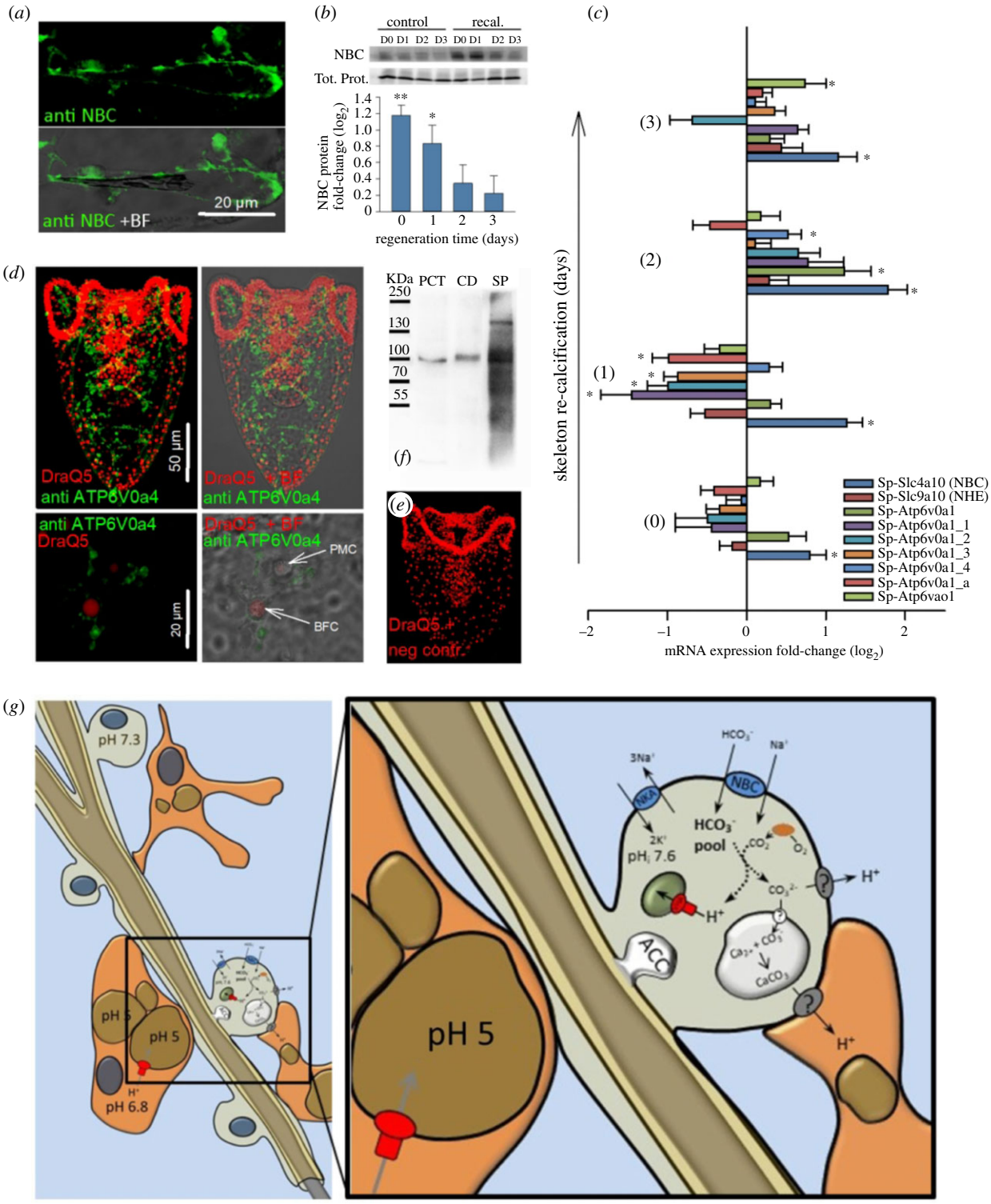

Figure 4. Modulation of acid–base transporters during skeleton re-calcification. (*a*) Immunolocalization of the Na^+/HCO_3^- cotransporter (NBC; Sp_Slc4a10) in re-calcifying PMCs. (*b*) Determination of NBC protein concentration during 4 days of skeleton re-calcification compared to control larvae that were not exposed to the low pH treatment. NBC protein levels were normalized to the total protein intensities. (*c*) qPCR analyses of *NBC* and *NHE* (*Sp_Slc9a2*) as well as the seven H^+-ATPase V0 isoforms identified in the sea urchin genome. Values are expressed as fold-change (log_2) relative to control larvae. (*d*) Positive immunoreactivity of the mammalian *ATPV0a4* antibody (kindly provided by Dr Carsten Wagner/Dr Soline Bourgeois) in sub-cellular vesicles of blastocoelar filopodial cells during skeleton re-calcification (D2) (green) and DraQ5 as a counterstain for nuclei (red). Negative controls were performed by omitting the primary antibody (*e*). Western blot performed with samples from mouse PCT, CD and whole larvae from *S. purpuratus* (SP) using the ATP6V0a4 antibody (*f*). Values are presented as mean ± s.e.m. ($n = 3$–6). Asterisks denote significant differences (**$p < 0.001$; *$p < 0.05$) between treatments. (*g*) Schematic summary of cellular processes in PMCs and blastocoelar filopodial cells (BFCs) during skeleton re-calcification in the sea urchin larva. (Online version in colour.)

VHA V0 subunit isoforms. While the majority, including *Sp_ATP6V0a1_1*, *a1_2*, *a1_3* and *a1_a* were significantly down-regulated at the time point of d1 an upregulation pattern with significant increases in *ATP6V0a1*, *a1_4* and *ao1* transcripts were found at the later time points of D2-3 (figure 4*c*). Using a polyclonal antibody raised against the V0 subunit of the human ATP6V0a4 protein, strong immunoreactivity was found in BFCs during re-calcification (D2) (figure 4*d*, upper panel). At a higher magnification, immunoreactivity was localized to sub-cellular structures surrounding the nucleus (red)

and within filopodial extensions of BFC (figure 4*d* lower panel). These vesicle-enriched filopodia come in close contact to PMCs that have no positive immunoreactivity to this antibody. Negative controls performed by omitting the primary antibody demonstrated specific binding of the secondary to the primary antibody (figure 4*e*). Western blot analyses demonstrate specific immunoreactivity of the ATP6V0a4 antibody with a 116 kDa protein in samples from mouse proximal convoluted tubules (PCT) and collecting duct (CD) as well as in extracts from *S. purpuratus* larvae (SP) (figure 4*f*). In addition to the 116 kDa band found in all samples the sea urchin homogenates had a second band with higher molecular mass of *ca* 150 kDa. The findings demonstrated a stimulation of bicarbonate transport by Slc4a10 in PMCs accompanied by increased H^+ transport capacity by multiple VHA isoforms during skeleton re-mineralization.

3. Discussion

(a) pH_i regulatory states of primary mesenchyme cells

The first set of experiments addressed the presence and role of proton transporting enzymes, including NHEs and VHAs in pH_i regulatory capacities of PMCs. Interestingly, PMCs within one larva responded with different sensitivities to EIPA. Calcein pulse-chase experiments of the present work in combination with the NHE inhibitor EIPA suggest a moderate (10–20%) EIPA sensitive incorporation of Ca^{2+} mainly in the mid-region of the primary rods, while Ca^{2+} incorporation is less affected in the aboral tips of the spicule. It seems that different PMCs have a different function that is related to their position along the body rods. The ones at the tip use EIPA insensitive mechanisms for calcification while the ones located away from the tips show EIPA sensitive incorporation of Ca^{2+}. This strongly correlates with the observation that PMCs have different functions in the normal calcification process where calcification is promoted at the tips and inhibited along the rods [28]. Further evidence for different functional states of PMCs is provided by *in situ* hybridization analyses in combination with calcein pulse-chase experiments [29]. Here, different expression levels of calcification related genes between cell bodies within one PMC syncytium were associated with differences in Ca^{2+} incorporation rates at distinct locations within the larval skeleton [29]. These findings in the sea urchin larva resemble those of mammalian systems, where two functional states of osteoblasts were identified [30]. Inactive osteoblasts form a thin epithelium lining the bone whereas active cuboidal osteoblasts are only found in active bone mineralizing regions expressing high concentrations of NHE-1 in basolateral membranes. These analogies suggest that also in the sea urchin larva, the formation of an elaborate skeleton is associated with a dynamic modulation of functional states in mineralizing PMCs.

In situ hybridization experiments demonstrated expression of *NHE* (*Sp_SLC9a2*) in PMCs [17] and our *S. purpuratus* specific Sp_Slc9a2 antibody confirms strong immunoreactivity with PMCs. NHEs have been associated with calcifying cells from algae [2] invertebrates [31] and mammals [18] with a predominant localization in the plasma membrane. In mineralizing osteoblasts the concept of proton removal by NHEs is supported by the upregulation of *NHE1* and *6* during mineralization [18]. By contrast, the present work did not find a substantial change in *Sp_Slc9a2* mRNA levels during skeleton re-calcification. Although the genetic basis remains unresolved, our pharmacological and biochemical studies demonstrated that NHEs are part of the pH regulatory machinery of PMCs. However, our results also demonstrate that Na^+/H^+ exchange activity mainly serves pH_i regulatory processes of PMCs during maintenance of the skeleton with only a minor contribution to the calcification process.

(b) pH_i regulatory dynamics of primary mesenchyme cells during skeleton re-calcification

Decalcification experiments of the present work confirmed earlier studies demonstrating the ability of sea urchin larvae to fully re-calcify their calcitic endoskeleton after dissolution by acidic conditions [32]. This assay was used to stimulate calcification rates of PMCs allowing us to study pH regulatory capacities and mechanisms of PMCs during active calcification. The re-calcification phase was accompanied by substantial changes in pH_i regulatory abilities of PMCs. Against our initial hypothesis that pH_i regulatory abilities should be increased during the re-calcification process, we found them to be dramatically decreased. However, during this phase, intracellular pH and $[HCO_3^-]$ levels were increased supporting the concept of substrate accumulation during an extensive re-mineralization event. This observation is supported by the substantial increase of *NBC* (*Sp_SLC4a10*) on the mRNA and the protein level, as well as an inhibition of cellular HCO_3^- transport by DIDS. Similar observations were made in human osteoblasts, that elevate pH_i from 6.62 to 7.35 when switching from a non-mineralizing to a mineralizing mode [30]. However, mineralizing osteoblasts increase pH_i regulatory capacities accompanied by an upregulation of *NHE1* and *NHE6* mRNA levels [18]. By contrast, PMCs reduce pH_i regulatory capacities and become insensitive to the Na^+/H^+ exchange inhibitor EIPA, suggesting a reduction in NHE-based pH regulatory capacities during skeleton re-calcification. Although decreased proton extrusion capacities of PMCs during active mineralization seem counterintuitive, low pH regulatory abilities of calcifying cells have been documented for other marine organisms. In the coccolithophore *Emiliania huxleyi*, decreases in seawater pH led to an uncompensated intracellular acidification [33]. OA simulations demonstrated that increases in environmental pCO_2 reduce pH_i of calicoblastic cells in three hermatypic coral species in an uncompensated manner [34]. Based on these observations and findings of the present work it can be concluded that cellular DIC accumulation is strongly stimulated during skeleton re-calcification. However, unlike the situation in vertebrates where the acid-load generated by the mineralization process is compensated by increased NHE activity, PMCs seem to use another route to remove protons from the calcification front.

(c) Vesicular proton accumulation during skeleton re-calcification

In a next step, we investigated the potential role of vesicular acid sequestration as an alternative route to locally remove protons from the cytosol. Intravesicular pH measurements demonstrated the presence of acidic (33%), neutral (15%) and alkaline (52%) vesicles in PMCs of the pluteus larvae. This endocytotic uptake of seawater-like fluids from the primary body cavity and subsequent vesicular acidification demonstrates a local, sub-cellular sequestration of protons

from the cytosol. Furthermore, during re-calcification of the larval skeleton, the number of large BFCs largely increase in the extracellular matrix of the primary body cavity that fuse with one another and connect to PMCs. These BFCs move with high velocities within the extracellular matrix and exchange large endocytosed acidic vesicles along their extensive filopodial network. These findings are consistent to earlier observations that described large multinucleated blastocoelar cells mainly during the phase of skeleton formation [35,36]. Analyses of cell fusion specificities using fluorescently labelled cells indicated that PMCs and blastocoelar cells (other mesenchyme cells) remain fusion competent along the larval development. However, this study also concluded that fusion-competent blastocoelar cells and PMCs come in contact but do not fuse with one another [35]. This observation is corroborated by our time-lapse recordings that demonstrated extensive trafficking of vesicles in filopodial networks but probably no direct transfer of vesicles from PMCs to BFCs. A comparison of PMCs and BFCs demonstrated substantially reduced pH regulatory capacities during skeleton re-calcification while those of BFCs resemble those of PMCs in a non-re-mineralizing mode. This difference in pH_i regulation of PMCs and BFCs further underline different functions of these two cell types during skeleton re-mineralization. Finally, acidification of large (diam. >1 µm) endocytotic vesicles within BFCs is sensitive to the VHA inhibitor Bafilomycin that also efficiently inhibits re-calcification of the larval skeleton. Here, it remains speculative if protons sequestered in these large vesicles derive from the calcification process or have another origin. These experiments indicate a critical involvement of the *V*-type ATPase during the process of skeleton re-calcification with the underlying mechanisms remaining speculative.

The VHA has been associated with the biomineralization process of different species including foraminifera [37], coccolitophores [38], cnidarians [39], molluscs [40,41] and crustaceans [42]. In foraminifera (*Ammonia* sp.), increased Bafilomycin-sensitive proton secretion has been demonstrated during chamber formation using the pH sensitive dye HPTS [37]. In the coccolithophore *E. huxleyi* gene expression studies [38], biochemical analyses [43] and flux modelling [44] suggested that besides a direct exit of H^+ through a voltage gated H^+ channel [45] calcification-derived protons are sequestered into sub-cellular compartments by a VHA. Screening of the seven VHA V_0 subunits found in the sea urchin revealed an upregulation of the *Sp_ATP6V0a1*, *Sp_ATP6V0a1_4* and *Sp_ATP6V0ao1* genes during re-calcification of the larval skeleton. Among these three isoforms of the V_0 subunit *Sp_ATP6V0a1* and *Sp_ATP6V0a1_4* are expressed by PMCs [46] and together with our pharmacological observations lends strong evidence for a key role of the V-ATPase in the mineralization process of the sea urchin larva. In addition, using an antibody designed against the mammalian ATP6V0a4, a strong immunoreactivity was detected in vesicular structures of BFCs corroborating our pharmacological inhibition of vesicular acidification in this cell type. Here, it remains unresolved which of the VHA isoforms is responsible for the massive sequestration of protons in BFCs and what the biological function may be. It can be speculated that this massive transport of protons into vesicular structures of BFCs is associated with a removal of protons liberated by the calcification process. Acidic vesicles may then be exocytosed into the primary body cavity or transported through the filopodial network to be released into the seawater at the highly permeable ectoderm. Furthermore, besides the possibility of direct secretion, vesicular sequestration of protons may also serve other cellular functions like enhanced protein degradation and processing in acidic lysosomes or autophagosomes during skeleton re-calcification [47].

4. Conclusion

By contrast to the situation in vertebrate osteoblasts, mineralizing cells of the sea urchin embryo reduce NHE-based pH_i regulatory capacities during extensive calcification events. However, the necessity to remove protons liberated by the calcification process suggests an alternative route of proton removal from the calcification front in PMCs. Here our vesicular pH measurements demonstrate a sub-cellular sequestration of protons in PMCs and BFCs potentially supporting pH_i regulation during the calcification process (figure 4*g*). It remains a matter of future investigations whether acidic vesicles in PMCs are exocytosed into the primary body cavity or if they can be transferred from PMCs to BFCs to be secreted or used for other cellular processes during skeleton repair (depicted by question marks in figure 4*g*). Despite these open questions regarding the removal of protons from the calcification front our results clearly demonstrate efficient cellular mechanisms of DIC accumulation during the mineralization event. Accordingly, reductions in seawater pH and carbonate saturation state as predicted for the coming century (Intergovernmental Panel on Climate Change) may represent a challenge for calcifying systems associated with low pH_i regulatory abilities, as changes in environmental pH directly interfere with cellular pH homeostasis. However, the findings of the present work also indicate that mineralization of the skeleton in the sea urchin larva underlies tight cellular control in terms of HCO_3^- acquisition and potential sub-cellular proton removal strategies that may counter ongoing changes in seawater carbonate chemistry. Here, the present work provides important mechanistic insights and new concepts for understanding the mineralization process in the sea urchin larva with strong implications for our interpretation of climate change effects on marine calcifiers.

5. Material and methods

(a) Experimental animals and re-calcification assay

Collection and culture of adult sea urchins (*S. purpuratus*), as well as preparation of larval cultures, was performed as previously described [19,48].

The re-calcification assay was performed as previously described by Pennington & Hadfield [32]. Briefly, larvae of *S. purpuratus* (3 dpf) were exposed to 0.03 M MES buffered FSW adjusted to pH 6.0 (FSW-pH 6). To fully dissolve the endoskeleton, larvae were exposed to FSW-pH 6.0 for 12–15 h. To regenerate their skeletons, larvae were transferred back into FSW (pH 8.0). The day of transfer back into FSW (pH 8.0) was defined as day 0 (D0), while the following days are consecutively numbered as D1, D2, D3, D4 and D6.

(b) Intracellular pH measurements

pH_i determinations and ammonia pulse experiments were conducted as previously described using the ratiometric membrane-permeable pH-sensitive dye 2′,7′-Bis-(2-carboxyethyl)-5-(and-6)-Carboxyfuorescein, Acetoxymethyl Ester (BCECF-AM) [15]. Control and re-calcifying larvae were measured in an alternate mode and from each larva 5–6 cells were simultaneously

recorded and treated as one replicate ($n = 1$). The CO_2 pulse technique was performed according to Suffrian *et al*. [33]. A detailed description of the experimental procedures is presented in the electronic supplementary material.

(c) Vesicular pH measurements

The membrane-impermeable pH-sensitive dye BCECF-FA 10 kDa dextran was used to monitor vesicular pH (pH_{Ves}). Control or re-calcifying larvae were incubated in BCECF-FA 10 kDa at a final concentration of 500 µM for 48 h. For vesicular pH recordings the ectoderm was removed according to the previously described 'bag isolation protocol' [15,49]. Ratiometric fluorescence recordings were performed on an inverted microscope using a 100× oil objective. To translate fluorescence intensity ratios into pH values, PMCs were exposed to an artificial seawater solution containing 10 µM Nigericin in combination with high external [K^+] (150 mM) (for details see [15]). This calibration solution allowed the calibration of pH_{VES} with our detected emission ratio of BCECF-FA in vesicles of living PMCs.

(d) Immunohistology and westernblot analysis

Immunofluorescence and western blot analysis was performed as previously described [19,48]. Polyclonal primary antibodies used in this study were generated against synthetic peptides corresponding to a carboxy-terminal region (CHGHHWIKEKWEEVNHK) of the sea urchin Sp_Slc9a2 protein and the sea urchin Na^+/HCO_3^- transporter Sp_SLC4a10 (for detailed information on Sp_SLC4a10 antibody validation see [17]). In addition a mammalian ATP6V0a4 antibody [50] was used to localize the ATP6V0 subunit in sea urchin larvae. Detailed information for immunohstochemical and western blot analyses are presented in the electronic supplementary material.

(e) Microinjection of reporter constructs and time-lapse imaging

Micro injections were performed as previously described [17]. The *alx1* BAC reporter construct (*Sp_BAC_042I08_L*) was obtained from the *S. purpuratus* BAC clone library (http://www.echinobase.org/Echinobase/bac_table/bac_table.php). BAC-GFP constructs were injected at a concentration of 25 ng μl^{-1} using a microinjection system (Picospritzer III, Parker) mounted on an inverse microscope (Zeiss ObserverD1) equipped with a cooling stage. *Alx1 BAC-GFP* injected larvae were raised for 3 days and then subjected to the decalcification procedure (see above). During re-calcification, larvae were exposed to 500 µM Texas Red labelled 10 KDa Dextran that was absorbed into cells by endocytotis. For life-cell imaging of PMCs and blastocoelar cells, larvae were placed on microscopy slides suspended in filtered seawater and covered with glass coverslips supported by approximately 100 µm-thick fibers as spacers. Larvae were then imaged with a Zeiss LSM510 using a Plan Neofluar 40×/1.3 objective at 15°C and for time lapse, images were taken at intervals of 10 s.

(f) Real-time-quantitative polymerase chain reaction and molecular cloning

Real-time-qPCR and molecular cloning were performed as previously described [17]. Expression levels were normalized to the housekeeping gene *EF1a* (SPU_000595) and amplification primers used for qPCR analysis are listed in the electronic supplementary material, table S1.

(g) Statistical analyses

Data from inhibitor studies were analysed using paired *t*-tests (Student's *t*-test). All data were normally distributed and passed equal variance tests (Levene test). For the analyses of gene expression, protein concentrations as well as comparisons of calcein fluorescence intensities and pharmacological experiments, one-way ANOVA followed by Holm–Sidak *post hoc* test was used. Statistical analyses were conducted using SIGMA STAT 13 (Systat Software).

Data accessibility. The data of this work are deposited in the Dryad Digital Repository: https://doi.org/10.5061/dryad.ngf1vhhrw [51].

Authors' contributions. M.Y.H. designed the study conducted experiments analysed data and wrote the manuscript. I.P. conducted intracellular pH measurements, immunohistochemcal analyses, analysed data and wrote the manuscript. W.W.C. conducted gene expression analyses and immunohistochemical analyses. C.B. performed and analysed intracellular pH measurements and pharmacological experiments. M.S. designed experiments analysed data and wrote the manuscript.

Competing interests. We declare we have no competing interests.

Funding. This study was funded by the Emmy-Noether-Programme (2611/1-1) of the Deutsche-Forschungs-Gesellschaft (DFG) to M.Y.H.

Acknowledgements. The authors would like to thank C. Wagner and Soline Bourgeois for kind provision of the ATP6V0a4 antibody and R. Lingg for assistance with western blot analyses.

References

1. Sikes CS, Okazaki K, Fink RD. 1981 Respiratory CO_2 and the supply of inorganic carbon for calcification of sea urchin embryos. *Comp. Biochem. Physiol. A Physiol.* **70**, 285–291. (doi:10.1016/0300-9629(81)90181-X)
2. Taylor AR, Brownlee C, Wheeler GS. 2017 Coccolitophore cell biology: chalking up progress. *Ann. Rev. Mar. Sci.* **9**, 283–310. (doi:10.1146/annurev-marine-122414-034032)
3. Vidavsky N, Addadi S, Schertel A, Ben-Ezra D, Shpigel M, Addadi L, Weiner S. 2016 Calcium transport into the cells of the sea urchin larva in relation to spicule formation. *Proc. Natl Acad. Sci. USA* **113**, 12 637–12 642. (doi:10.1073/pnas.1612017113)
4. IPCC. 2014 IPCC 2014: climate change 2014: synthesis report. Contribution of Working groups I, II; III to the fifth assessment report of the intergovernmental panel on climate change. Geneva, Switzerland: IPCC.
5. Wilt FH. 2002 Biomineralization of the spicules of sea urchin embryos. *Zoolog. Sci.* **19**, 253–261. (doi:10.2108/zsj.19.253)
6. Théel H. 1892 On the development of *Echinocyamus pusillus* (O. F. Müller). *Nova Acta R. Soc. Sci. Upsal Ser. III* **15**, 1–57.
7. Shashikant T, Kohr JM, Ettensohn CA. 2018 From genome to anatomy: the architecture and evolution of the skeletogenic gene regulatory network of sea urchins and other echinoderms. *Genesis* **56**, e23253. (doi:10.1002/dvg.23253)
8. Decker G, Lennartz WJ. 1988 Skeletogenesis in the sea urchin embryo. *Development* **103**, 231–247.
9. Morgulis M *et al.* 2019 Possible cooption of a VEGF-dricen tubulogenesis program for biomineralization in echinoderms. *Proc. Natl Acad. Sci. USA* **116**, 12 353–12 362. (doi:10.1073/pnas.1902126116)
10. Beniash E, Aizenberg J, Addadi L, Weiner S. 1997 Amorphous calcium carbonate transforms into calcite during sea urchin larval spicule growth. *Proc. R. Soc. Lond. B* **264**, 461–465. (doi:10.1098/rspb.1997.0066)
11. Vidavsky N, Addadi S, Mahamid J, Shimoni E, Ben-Ezra D, Shpigel M, Weiner S, Addadi L. 2014 Initial stages of calcium uptake and mineral deposition in sea urchin embryos. *Proc. Natl Acad. Sci. USA* **111**, 39–44. (doi:10.1073/pnas.1312833110)
12. Beaniash E, Adadi L, Weiner S. 1999 Cellular control over spicule formation in sea urchin embryos: a

structural approach. *J. Struct. Biol.* **125**, 50–62. (doi:10.1006/jsbi.1998.4081)

13. Benson SC, Benson NC, Wilt FH. 1986 The organic matrix of the skeletal spicule of sea urchin embryos. *J. Cell Biol.* **102**, 1878–1886. (doi:10.1083/jcb.102.5.1878)
14. Jain G, Pendola M, Rao A, Cölfen H, Evans JS. 2016 A model sea urchin spicule matrix protein self-associates to form mineral-modifying hydrogels. *J. Struct. Biol.* **183**, 205–215.
15. Stumpp M *et al.* 2012 Acidified seawater impacts sea urchin larvae pH regulatory systems relevant for calcification. *Proc. Natl Acad. Sci. USA* **109**, 18 192–18 197. (doi:10.1073/pnas.1209174109)
16. Killian CE, Wilt FH. 2017 Endocytosis in primary mesenchyme cells during sea urchin larval skeletogenesis. *Exp. Cell Res.* **359**, 205–214. (doi:10.1016/j.yexcr.2017.07.028)
17. Hu MY, Yan J-J, Petersen I, Himmerkus N, Bleich M, Stumpp M. 2018 A Slc4 family bicarbonate transporter is critical for intracellular pH regulation and biomineralization in sea urchin embryos. *Elife* **7**, e36600. (doi:10.7554/eLife.36600)
18. Liu L, Schlesinger PH, Slack NM, Friedmann PA, Blair HC. 2011 High capacity Na^+/H^+exchange activity in mineralizing osteoblasts. *J. Cell. Physiol.* **226**, 1702–1712. (doi:10.1002/jcp.22501)
19. Stumpp M, Hu MY, Tseng Y-C, Guh YJ, Chen YC, Yu JK, Su YH, Hwang PP. 2015 Evolution of extreme stomach pH in bilateria inferred from gastric alkalization mechanisms in basal deuterostomes. *Sci. Rep.* **5**, 1–9. (doi:10.1038/srep10421)
20. Schatzberg D, Lawton M, Hadyniak SE, Ross EJ, Carney T, Beane WS, Levin M, Bradham CA. 2015 H^+/K^+-ATPase activity is required for biomineralization in sea urchin embryos. *Dev. Biol.* **406**, 259–270. (doi:10.1016/j.ydbio.2015.08.014)
21. Rafiq K, Shashikant T, McManus CJ, Ettensohn CA. 2014 Genome-wide analysis of the skeletogenic gene regulatory network of sea urchins. *Development* **141**, 950–961. (doi:10.1242/dev.105585)
22. Lee H-G, Stumpp M, Yan J-J, Tseng Y-C, Heinzel S, Hu MY. 2019 Tipping points of gastric pH regulation and energetics in the sea urchin larva exposed to CO_2-induced seawater acidification. *Comp. Biochem. Physiol. A Mol. Integr. Physiol.* **234**, 87–97. (doi:10.1016/j.cbpa.2019.04.018)
23. Tu Q, Cameron RA, Davidson EH. 2014 Quantitative developmental transcriptomes of the sea urchin *Strongylocentrotus purpuratus*. *Dev. Biol.* **385**, 160–167. (doi:10.1016/j.ydbio.2013.11.019)
24. Damle S, Davidson EH. 2011 Precise *cis*-regulatory control of spacial and temporal expression of the *alx-1* gene in the skeletogenic lineage of *S. purpuratus*. *Dev. Biol.* **357**, 505–517. (doi:10.1016/j.ydbio.2011.06.016)
25. Ettensohn CA, Illies M, Olivieri P, De Jong DL. 2003 Alx1, a member of the Cart1/Alx3/Alx4 subfamily of Paired-class homedomain proteins, is an essential component of the gene network controlling skeletogenic fate specification in the sea urchin embryo. *Development* **130**, 2917–2928. (doi:10.1242/dev.00511)
26. Ivanov AI. 2008 Pharmacological inhibition of endocytic pathways: is it specific enough to be useful? *Methods Mol. Biol.* **440**, 15–33. (doi:10.1007/978-1-59745-178-9_2)
27. Pörtner HO, Boutilier RG, Toews DP. 1990 Determination of intracellular pH and pCO_2 after metabolic inhibition by fluoride and nitrilotriacetic acid. *Respir. Physiol.* **81**, 255–273. (doi:10.1016/0034-5687(90)90050-9)
28. Sun Z, Ettensohn CA. 2014 Signal-dependent regulation of the sea urchin skeletogenic gene regulatory network. *Gene Expr. Patterns* **16**, 93–103. (doi:10.1016/j.gep.2014.10.002)
29. Guss KA, Ettensohn CA. 1997 Skeletal morphogenesis in the sea urchin embryo: regulation of primary mesenchyme gene expression and skeletal rod growth by ectoderm-derived cues. *Development* **124**, 1899–1908.
30. Blair HC, Larrouture QC, Tourkova IL, Liu L, Bian JH, Stolz DB, Nelson DJ, Schlesinger PH. 2018 Support of bone mineral deposition by regulation of pH. *Am. J. Physiol. Cell Physiol.* **315**, C587–C597. (doi:10.1152/ajpcell.00056.2018)
31. Ahearn GA, Mandal P, Mandal A. 2001 Biology of the $2Na^+/1H^+$ antiporter in invertebrates. *J. Exp. Zool.* **289**, 232–244. (doi:10.1002/1097-010X(20010401/30)289:4<232::AID-JEZ4>3.0.CO;2-T)
32. Pennington JT, Strathmann RR. 1990 Consequences of the calcite skeletons of planktonic echinoderm larvae for orientation, swimming, and shape. *Biol. Bull.* **179**, 121–133. (doi:10.2307/1541746)
33. Suffrian K, Schulz KG, Gutowska MA, Riebesell U, Bleich M. 2011 Cellular pH measurements in *Emiliania huxleyi* reveal pronounced membrane proton permeability. *New Phytol.* **190**, 595–608. (doi:10.1111/j.1469-8137.2010.03633.x)
34. Venn AA, Tambutté E, Caminiti-Segonds N, Techer N, Allemand D, Tambutté S. 2019 Effects of light and darkness on pH regulation in three coral species exposed to seawater acidification. *Sci. Rep.* **9**, 2201. (doi:10.1038/s41598-018-38168-0)
35. Hodor PG, Ettensohn CA. 1998 The dynamics and regulation of mesenchymal cell fusion in the sea urchin embryo. *Dev. Biol.* **199**, 111–124. (doi:10.1006/dbio.1998.8924)
36. Gustafson T, Wolpert L. 1967 Cellular movement and contact in sea urchin morphogenesis. *Biol. Rev.* **42**, 442–498. (doi:10.1111/j.1469-185X.1967.tb01482.x)
37. Toyofuku T *et al.* 2017 Proton pumping accompanies calcification in foraminifera. *Nat. Commun.* **8**, 14145. (doi:10.1038/ncomms14145)
38. MacKinder L, Wheeler GS, Schroeder D, von Dassow P, Riebesell U, Brownlee C. 2011 Expression of biomineralization-related ion trnasport genes in *Emiliania huxleyi*. *Environ. Microbiol.* **13**, 3250–3265. (doi:10.1111/j.1462-2920.2011.02561.x)
39. Allemand D, Ferrier-Pagès C, Furla P, Houlbrèque F, Puverel S, Reynaud S, Tambutté E, Tambutté S, Zoccola D. 2004 Biomineralization in reef-building coral: from molecular mechanisms to environmental control. *C. R. Palevol.* **3**, 453–467. (doi:10.1016/j.crpv.2004.07.011)
40. Li S, Huang J, Liu C, Liu Y, Zheng G, Xie L, Zhang R. 2016 Interactive effects of seawater acidification and elevated temperature on the transcriptome and biomineralization in the pearl oyster *Pinctada fucata*. *Environ. Sci. Technol.* **50**, 1157–1165. (doi:10.1021/acs.est.5b05107)
41. Ivanina AV, Falfushynska HI, Beniash E, Piontkivska H, Sokolova IM. 2017 Biomineralization-related specialization of hemocytes and mantle tissue of the pacific oyster *Crassostrea gigas*. *J. Exp. Biol.* **220**, 3209–3221. (doi:10.1242/jeb.160861)
42. Ziegler A, Weihrauch D, Hagedorn M, Towle DW, Bleher R. 2004 Expression and polarity reversal of V-type H^+-ATPase during the mineralization-demineralization cycle in *Porcellio scaber* sternal epithelial cells. *J. Exp. Biol.* **207**, 1749–1756. (doi:10.1242/jeb.00953)
43. Corstjens PLAM, Araki Y, González EL. 2001 A coccolithophorid calcifying vesicle with a vacuolar-type ATPase proton pump: cloning and immunolocalization of the V0 subunit c. *J. Phycol.* **37**, 71–78. (doi:10.1046/j.1529-8817.1999.014012071.x)
44. Holtz LM, Thoms S, Langer G, Wolf-Gladrow DA. 2013 Substrate supply for calcite preparation in *Emiliania huxleyi*: assessment of different model approaches. *J. Phycol.* **49**, 417–426. (doi:10.1111/jpy.12052)
45. Taylor AR, Chrachri A, Wheeler GS, Goddard H, Brownlee C. 2011 A voltage-gated H^+ channel underlying pH homeostasis in calcifying coccolithophores. *PLoS Biol.* **9**, e1001085. (doi:10.1371/journal.pbio.1001085)
46. Zhu X, Mahairas G, Illies M, Cameron RA, Davidson EH, Ettensohn CA. 2001 A large-scale analysis of mRNAs expressed by primary mesenchyme cells of the sea urchin embryo. *Development* **128**, 2615–2627.
47. Maxon ME, Grinstein S. 2014 The vacuolar-type H^+-ATPase at a glance- more than a proton pump. *J. Cell Sci.* **127**, 4987–4993. (doi:10.1242/jcs.158550)
48. Stumpp M, Hu MY, Casties I, Saborowski R, Bleich M, Melzner F, Dupont ST. 2013 Digestion in sea urchin larvae impaired under ocean acidification. *Nat. Clim. Change* **3**, 1044–1049. (doi:10.1038/nclimate2028)
49. Harkey MA, Whiteley AH. 1980 Isolation, culture, and differentiation och echinoid primary mesenchyme cells. *Wilhelm Roux's Arch. Dev. Biol.* **189**, 111–122. (doi:10.1007/BF00848500)
50. Wagner CA, Lükewille U, Valles P, Breton S, Brown D, Giebisch GH, Geibel JP. 2003 A rapid enzymatic method for the isolation of defined kidney tubule fragments from mouse. *Pflügers Archiv Eur. J. Physiol.* **446**, 623–632. (doi:10.1007/s00424-003-1082-3)
51. Hu MY, Petersen I, Chang WW, Blutron C, Stumpp M. 2020 Data from: Cellular bicarbonate accumulation and vesicular proton transport promote calcification in the sea urchin larva. Dryad Digital Repository. (https://doi.org/10.5061/dryad.ngf1vhhrw)